A Novel Cellular Automata Modelling Framework for Micro-environmental Interaction and Co-invasion

Arran Hodgkinson[1,2(✉)]

[1] DIMNP, Université de Montpellier, 34095 Montpellier, France
[2] Institut de Recherche en Cancérologie de Montpellier, 34298 Montpellier, France
arran.hodgkinson@umontpellier.fr

Abstract. Modern biological paradigms of invasion in tumour cells cannot be fully explained or described by existing modelling techniques. We present a novel cellular automata model which represents both the nucleus of a cell and its membrane, allowing one to capture the interaction of a cell with its environment, as well as selected theorems for the efficient computation of solutions to such systems. We use this technique to simulate cell-cell binding, single-cellular micro track invasion, and co-injection of $\text{MITF}^{\text{HIGH}}$(proliferative) and MITF^{LOW}(invasive) tumour cells into heterogeneous environments. Results shed new light on emergent phenomena of cellular elongation, filopodial protrusion, and the co-invasion of the local stroma by classically non-invasive cells. We also provide a new modelling framework in which the cellular automaton exhibits non-local interaction within its context.

Keywords: Cellular automata · Mathematical modelling
Cellular biology · Coöperation · Numerical analysis

1 Introduction

Biological paradigms involving mixtures of heterogeneous subpopulations of cells have become the subject of increased scrutiny in recent years. Beginning from problems of cell sorting [5], cellular interactions now have a field of automata devoted to their exploration. One problem of significance is the change in behaviour of ordinarily non-invading proliferative cells ($\text{MITF}^{\text{HIGH}}$) in the presence of highly invasive, non-proliferative cells (MITF^{LOW}). Injection of these cellular populations, *in vivo*, in isolation yielded ordinary pathological behaviour whereas co-injection of disparate species led to the co-invasion of the local stroma by $\text{MITF}^{\text{HIGH}}$cells, on a substrate altered by leading MITF^{LOW}cells [4].

This also gives rise to more general problems in invasion. One methodology of cellular invasion involves the utilisation of 'microtracks', or spaces of reduced ECM concentration, by cells in order to gain a competitive advantage, travelling

Supported by l'École Doctorale I2S de l'Université de Montpellier.

G. Mauri et al. (Eds.): ACRI 2018, LNCS 11115, pp. 30–41, 2018.
https://doi.org/10.1007/978-3-319-99813-8_3

at increased speeds by direct comparison with those cells forced to travel through the dense ECM [2]. This increase in migration through native microtracks was shown, using time-lapse photography, to occur within the 3D collagen matrix. These microtracks have further been shown to have varying mean width and variance [8] which may be as a result of underlying matrix structuring and varying collagen densities across a given region. Importantly, the cells were shown to exhibit patterns of actin recruitment that were not discernible from those found in migratory cells out with microtracks [8].

The discrete Cellular Potts models which have been proposed model the cell moving through a grid-like structure, however fine, guided by a mechanistic, stochastic function [5]. Indeed, these have great power in reproducing qualitatively realistic results and can model even relatively complex systems [10]. These models exist in a discrete space where the implementation of behaviours is dependent on a delta probability function rather than the continuous machinery of the cell. This means that they lack the ability to, for example, explain or describe microtrack motility or to fully explain any emergent phenomena due to the model's reliance on stochastic dynamics.

One particular model which does not study the cell mechanics themselves, demonstrates that one can take a more physical interpretation of the tumour and its environment [11]. This model, again, chooses to describe a cellular population as a non-autonomous series of ball-like structures in arbitrary space acting under the standard forces (drag, traction, *et cetera*). The complexity of membrane-dependent biological interactions requires the creation of a novel cellular automata model who describes not only the position of the cells but endows them with some physical form which mediates its interaction with its environment.

In Sect. 2 of this paper, we begin to build the novel framework necessary to accurately capture these phenomena and the field equations which biologically contextualise the automata. We then provide, in Sect. 3, numerical analysis of approximations, necessary for the fast computation of results, to the modelling scheme in order to bound the errors for these approximations. Finally, in Sect. 4, we present the result of simulations for a small system of cellular automata in order to demonstrate their ability to elucidate biological cell invasion in heterogeneous colonies and environments.

2 A Novel Modelling Framework

Firstly, we choose to express the environmental system in standard Cartesian coordinates and the radial equations for the distance of the membrane from the nucleus in polar coordinates. We then have that the standard coordinate conversion from polar to Cartesian is given by $x = \mathbf{r}\cos\theta$, $y = \mathbf{r}\sin\theta$ and we write $\mathbf{x} := [x, y]^T$. Therefore, let $\mathcal{I} = [0, T)$ be the time domain on which the system exists and $\mathcal{D} \subseteq \mathbb{R}^2$ be the spatial domain.

Secondly, let $\mathbf{r}(t, \theta)$, be a 2π periodic function such that $\mathbf{r}(t, \theta + 2n\pi) = \mathbf{r}(t, \theta)$, $\forall n \in \mathbb{N}$, and let it further define the perimeter of a cell with the brief

notation $\mathbf{r} := \mathbf{r}(\theta) := \mathbf{r}(t, \theta)$. Let $\Theta = [0, 2\pi)$ be the domain for the nucleus-centred radius and let $\mathcal{R} \subseteq \mathbb{R}$ be the domain for the radius of the cell such that $\mathbf{r} : \mathcal{I} \times \Theta \to \mathcal{R}$. For cell i, we denote the radius $\mathbf{r}_i$. Finally, let $v : \mathcal{I} \times \mathcal{D} \to \mathbb{R}$ define the extracellular matrix (ECM) density and let $\mathbf{m} : \mathcal{I} \times \mathcal{D} \to \mathbb{R}^q$ define the q molecular species densities on the domain.

2.1 On Cell-Cell Bonding and Associated Field Equations

We begin by reposing every cell-cell interaction problem as a generic problem between two cells situated a given distance d from one another and with both of their respective centres at $y = 0$. First, let the vector $\mathbf{p}(c_i, c_j)$ be the vector in polar coordinates such that

$$||\mathbf{p}|| := \sqrt{(\bar{c}_{i,x} - \bar{c}_{j,x})^2 + (\bar{c}_{i,x} + \bar{c}_{j,x})^2}\,, \qquad \mathbf{p}_\theta := \tan^{-1}\left(\frac{\bar{c}_{j,y} - \bar{c}_{i,y}}{\bar{c}_{j,x} - \bar{c}_{i,x}}\right) \tag{1}$$

where $\bar{c}_i$ denotes the centre of mass for the cell c_i, then call this the pointing vector and perform the transforms $(r_j, \theta_j) \to \left(r_j, \theta_j - \mathbf{p}_\theta + \frac{\pi}{2}\right)$ and $(\bar{c}_{j,x}, \bar{c}_{j,y}) \to (0, ||\mathbf{p}||)$, in order to move cell j onto the x-axis and to rotate the cell such that the same points are aligned as was the case prior to the coordinate transform.

Then, from simple algebraic reasoning, one has that the distance between any two points on the membranes of these cells, with respect to θ, is given by

$$d(\theta) = \sqrt{(c_{i,r}\cos(\theta) - c_{j,r}\cos(\theta))^2 + (c_{i,r}\sin(\theta) - c_{j,r}\sin(-\theta) + ||\mathbf{p}||)^2} \tag{2}$$

and this means that the contribution to a given radius can be calculated by the force at that point, multiplied by the appropriate elongation factor which is given by the trigonometric relation $\bar{d} = d\cos\left(\theta - \frac{\pi}{2}\right)$, where $\frac{\pi}{2}$ is a factor which accounts for the reorientation of the cells.

Let us now look at the attractive intercellular force, $F_A(d)$. There is evidence to suggest that, below some limiting distance, the negative charges on repeat 3 of α-actinin and positive charges on intercellular adhesion molecule (ICAM)-1 dominate the interaction. Above this distance, the contribution of the positive-positive interaction is increased between the acidic centre of the α-actinin domain and Lys acids on ICAM1 [3,9]. We model this by introducing some constant imaginary distance, i, between the two membranes.

The repulsive Coulomb force, $F_R(d)$, emanates from the addition of pressure to the membrane reducing the spacing between membranous lipids, producing a restorative force. Therefore, we calculate the distance at which the centre of charge of the membrane sits, with respect to the cell radius. For a circle of uniform radius $r(\theta) = r$, the radial centre of charge is approximated by $\bar{r} \approx \frac{4}{3\pi}r$, which shall serve as a positioning of the internal charge.

We can then write the overall field equation as

$$F(d) = \frac{1}{(d - d_A)^2 + 1} - \frac{1}{\left(d + \frac{4}{3\pi}\right)^2 + \frac{1}{Q_s}} \tag{3}$$

where Q_s gives the ratio of charge separation for the protein complex, with respect to the separation of the charges in the lipid bilayer of the melanoma cells themselves. Biological precedents for this force distribution exists, with physical measurement being taken between staphylococcus aureus cells and biofilms [6].

2.2 On Cell-ECM Bonding and Associated Field Equations

The dissociation rate of one protein from another is widely considered [1,7] to have the form $k = k_0 \exp(fx/k_bT)$, where k_0 is the zero rate of dissociation, f is the force applied in separating the proteins, x is the distance of separation, and k_BT gives the thermal energy of the system. Now, consider an arbitrary force that brings the proteins of the cell and the ECM together, then their normalised association rate, $\bar{k}$, would be given by $\bar{k} = [1 - (k_0/K)\exp(-fx/k_bT)]$ where the maximal rate of dissociation is given by K.

The force on the cell from the ECM is proportional to the density of the ECM itself and therefore we write $|F_c^+| = \bar{k}v$. We also have that the direction of association is from lower to higher densities of protein, which follows directly from their proportionality. As for the force equation for pressure, we assume the field generated scales with the square of the ECM density, and acts in the opposite direction. Therefore, we can write the entirety of the force equation as

$$|F| = \left[1 - \frac{k_0}{K}\exp\left(-\frac{fx}{k_bT}\right)\right] v - k_P v^2\,, \qquad \hat{F} = \tan^{-1}\left(\frac{\partial v}{\partial y}\frac{\partial x}{\partial v}\right). \tag{4}$$

2.3 Molecular Species on the Boundary — Chemotaxis

The chemotaxis of a cell is dependent on the molecular species concentration $m(t,x)$ on the immediate boundary of the cell, since it is not endocytosis but simply sensory response that is necessary for this stimulus.

Using the standard definition of a line integral, we can write the line integral of the molecular species concentration $m_i(x,y)$ over the boundary of the cell and with surface element σ as

$$I = \int\limits_{\partial\Omega_i} m_i(\bar{x})\,d\sigma\,, \qquad d\sigma = \sqrt{\mathbf{r}(\theta)^2\sin^2\theta + \mathbf{r}(\theta)^2\cos^2\theta}\,d\theta = \mathbf{r}(\theta)\,d\theta\,. \tag{5}$$

It is then trivial to rewrite the line integral with respect to the individual cell and a specific molecular species, $m_j(t,x)$, to obtain the overall molecular species concentration on the boundary, and the bias of such a concentration.

Taking the biased molecular concentrations and extract from them the optimal direction, in terms of chemical attractants, the mean biased chemotaxis is given by

$$\overset{\circ}{\chi} = \frac{1}{\sum\limits_{j=1}^{q}\chi_{m_j}}\begin{pmatrix}\chi_{m_1}\\ \vdots \\ \chi_{m_q}\end{pmatrix}\cdot\begin{pmatrix}\tan^{-1}\left(\dfrac{\int_\Theta m_1(\mathbf{r}(\theta)\cos\theta,\mathbf{r}(\theta)\sin\theta)\cos\theta\,d\theta}{\int_\Theta m_1(\mathbf{r}(\theta)\cos\theta,\mathbf{r}(\theta)\sin\theta)\sin\theta\,d\theta}\right)\\ \vdots \\ \tan^{-1}\left(\dfrac{\int_\Theta m_q(\mathbf{r}(\theta)\cos\theta,\mathbf{r}(\theta)\sin\theta)\cos\theta\,d\theta}{\int_\Theta m_q(\mathbf{r}(\theta)\cos\theta,\mathbf{r}(\theta)\sin\theta)\sin\theta\,d\theta}\right)\end{pmatrix} \tag{6}$$

where the chemotactic constant for any given molecular species $m_j(t,x)$ is given by χ_{m_j}.

2.4 Temporal Changes in Intracellular Properties

We must, further, have a means by which the cell's interior can reposition itself with respect to the environment. A sensible candidate for this movement can simply be taken as a result of the net forces which move the membrane of the cell having direct and proportionate effect on the position of the nucleus such that we can write

$$\frac{\partial}{\partial t}x_1 = \int\limits_{[0,2\pi)} \frac{\partial}{\partial t}\mathbf{r}(\tilde{\theta}) \cdot \cos\tilde{\theta}\, d\tilde{\theta}\,, \qquad \frac{\partial}{\partial t}x_2 = \int\limits_{[0,2\pi)} \frac{\partial}{\partial t}\mathbf{r}(\tilde{\theta}) \cdot \sin\tilde{\theta}\, d\tilde{\theta}\,, \tag{7}$$

reflecting a mechanical movement of the nucleus with the membrane.

Consider the overall change in the polarisation, ϕ, of the cell and that the cell is capable of rearranging its internal infrastructure in response to the attraction of chemicals and in order to maximise its potential for utilising the byproducts of this infrastructure. Then we assume that the cell will attempt to reorient itself to the optimal direction

$$\bar{\phi} = \frac{1}{\omega_F + \omega_\chi}\left(\omega_F \tan^{-1}\left(\frac{\partial x_2}{\partial t}\frac{\partial t}{\partial x_1}\right) + \omega_\chi \overset{\circ}{\chi}\right), \tag{8}$$

given the weightings ω_F, ω_χ for the force and chemotactically mediated polarity preferences, respectively.

Then consider that the cell will have more success in achieving small angular reorientation than in large angular reorientations. Therefore, we make the assumption that the polarisation may only change through small changes around the perimeter of the cell and that $\ln(\partial\phi/\partial t) \propto -\left(\bar{\phi} - \phi\right)^2$. We write that the change in polarisation can be given by

$$\frac{\partial \phi}{\partial t} = \exp\left[-\left(\left(\frac{\partial x_1}{\partial t}\right)^2 + \left(\frac{\partial x_2}{\partial t}\right)^2\right)^{-\frac{1}{2}} \cdot \left(\bar{\phi} - \phi\right)^2\right]. \tag{9}$$

3 Numerical Approach

3.1 Movement of the Nucleus: A Simple Translation Method

The current methodology for reassignment, or mathematical translation, of the position of a radial function $\mathbf{r}(\theta)$ to a differing position is given as follows

$$\mathbf{r}_1 = \sqrt{\mathbf{r}^2 + \mathbf{r}_0^2 + 2\mathbf{r}\mathbf{r}_0\cos(\theta_0 - \theta)}\,, \qquad \theta_1 = \cos^{-1}\left(\frac{\mathbf{r}\cos\theta + \mathbf{r}_0\cos\theta_0}{\mathbf{r}_1}\right), \tag{10}$$

where $(\mathbf{r}, \theta)$ gives the original solution in polar coordinates; $(\mathbf{r}_0, \theta_0)$ gives the magnitude and direction of the translation; and $(\mathbf{r}_1, \theta_1)$ gives the translated set of solutions. Then observe the following simplification:

Theorem 1. *Let the space $\mathcal{N} \subseteq \mathbb{R}^2$ define the Cartesian plane on which the nucleus of a given 2-dimensional cell is defined, and the space $\mathcal{Q} \subseteq \mathbb{R} \times [0, 2\pi)$ define the polar domain centred at $(x, y) \in \mathcal{N}$ on which the membrane of the cell is defined. Then we can define a cell as some $[(x_0, y_0), (\mathbf{r}_0(\theta_0), \theta_0)] \in \mathcal{N} \times \mathcal{Q}$, where $\mathbf{r}(\theta) : [0, 2\pi) \to \mathbb{R}$ is the radial membrane distance as measured from the centre of the cell. Define further a formula for translation of the nucleus of this cell, given by $(x, y) \to (x + \xi, y)$, where the membrane of the cell retains its position in the cartesian space and dependence on θ_0, given by*

$$\mathbf{r}_1(\theta_0) = \mathbf{r}_0(\theta_0) - \xi \cos(\theta_0)\,.$$

Then the error for this translation is given by

$$E_r \leq \left(1 - \sin\left(\frac{1}{2}\cos^{-1}\left(\frac{-\mathbf{r}(\hat{\theta}) + \sqrt{\mathbf{r}(\hat{\theta})^2 + 8\xi^2}}{4\xi}\right)\right)\right)\left(\frac{-\mathbf{r}(\hat{\theta}) + \sqrt{\mathbf{r}(\hat{\theta})^2 + 8\xi^2}}{4\xi}\right)\xi,$$

where $\mathbf{r}(\hat{\theta}) = \max\limits_{\theta \in [0,2\pi)} \mathbf{r}(\theta)$.

Proof. Recall the coordinate relations given by $x_0 = \mathbf{r}(\theta)\cos\theta$, $y_0 = \mathbf{r}(\theta)\sin\theta$ and the counter-relation $\mathbf{r}(\theta)^2 = x^2 + y^2$. Consider, further, the translation in only the cartesian x-direction, of magnitude ξ, corresponding to a linear progression in an aligned set of polar axes given by $x_1 = \mathbf{r}(\theta)\cos\theta - \xi$, $y_1 = \mathbf{r}(\theta)\sin\theta$.

Using the translation approximation $\mathbf{r}_1(\theta_0) = \mathbf{r}_0(\theta_0) - \xi\cos(\theta_0)$ and allowing that the maximal error for this approximation is given at $\theta_0 = \hat{\theta}$, defined by $\mathbf{r}(\hat{\theta}) := \max\limits_{\theta \in [0,2\pi)} \mathbf{r}(\theta)$, the maximal error is given by

$$\bar{E} = \underbrace{(\mathbf{r}(\hat{\theta}) + \xi\cos\hat{\theta})\sin\hat{\theta}}_{\text{approximation}} - \underbrace{(\mathbf{r}(\hat{\theta})^2 - (\mathbf{r}(\hat{\theta})\sin\hat{\theta} - \xi)^2)^{\frac{1}{2}}}_{\text{absolute calculation}}\,. \tag{11}$$

We can then find this maximum at $\hat{\theta}$ by considering the derivative of the term for the translation approximation, which simplifies to

$$\tilde{E}' = \mathbf{r}(\hat{\theta})\cos\hat{\theta} + \xi\cos 2\hat{\theta} = 0 \tag{12}$$

and by further using the trigonometric relation $\cos 2\theta = 2\cos^2\theta - 1$ we can write

$$\mathbf{r}(\hat{\theta})\cos\hat{\theta} + 2\xi\cos^2\hat{\theta} - \xi = 0 \tag{13}$$

who is a quadratic in $\cos\hat{\theta}$, such that the solution for $\hat{\theta}$ is given by

$$\cos\hat{\theta} = \frac{-\mathbf{r}(\hat{\theta}) \pm \sqrt{\mathbf{r}(\hat{\theta})^2 + 8\xi^2}}{4\xi} \quad \Longrightarrow \quad \hat{\theta} = \cos^{-1}\left(\frac{-\mathbf{r}(\hat{\theta}) + \sqrt{\mathbf{r}(\hat{\theta})^2 + 8\xi^2}}{4\xi}\right). \tag{14}$$

Substituting this into the original equation, and recognising that the negative term in the error is minimised at $x = \xi$, one has that the maximal error is written

$$\bar{E} = \mathbf{r}\left(\cos^{-1}\left(\frac{-\mathbf{r}(\hat{\theta}) + \sqrt{\mathbf{r}(\hat{\theta})^2 + 8\xi^2}}{4\xi}\right)\right) + \left(\frac{-\mathbf{r}(\hat{\theta}) + \sqrt{\mathbf{r}(\hat{\theta})^2 + 8\xi^2}}{4\xi}\right)\xi - \mathbf{r}(\hat{\theta})\,. \tag{15}$$

Then the precise value of $y(\hat{\tilde{\theta}})$ is given at $y(\hat{\tilde{\theta}}) = \mathbf{r}(\frac{1}{2}\hat{\theta})\sin(\frac{1}{2}\hat{\theta})$, such that the maximal error can be given precisely by

$$\bar{E} = \left(1 - \sin\left(\frac{1}{2}\cos^{-1}\left(\frac{-\mathbf{r}(\hat{\theta}) + \sqrt{\mathbf{r}(\hat{\theta})^2 + 8\xi^2}}{4\xi}\right)\right)\right)\left(\frac{-\mathbf{r}(\hat{\theta}) + \sqrt{\mathbf{r}(\hat{\theta})^2 + 8\xi^2}}{4\xi}\right)\xi. \tag{16}$$

In this case, using Theorem 1, the error for values of $\xi \leq 0.1$ is such that $E_r < \frac{1}{2}\xi^2$ and ξ is proportional with the time step such that $\xi \propto \delta\tau$. Thus, for sufficiently small time steps one is able to discern that the error is sufficiently small, and non-cumulative, and that this may be acceptable within the bounds of expected numerical error.

3.2 Numerical Approximations of Line Integrals

We begin by recalling that the analytic, single-variable line integral for a radial function is given by $I = \int_{\mathcal{S}} r(\theta)\, d\sigma$, where $\mathcal{S}$ is used to denote the surface of the cell and σ is some surface element on $\mathcal{S}$. Discretisation of this system leads us to derive a metric on the basis of maximal efficacy on the discrete radial interval, $(\tilde{\theta}, \tilde{\theta} + \delta\theta)$. Begin by considering the true arc length in this portion of the radius of a given cell and notice that this can be approximated by sketching a line between the two extreme radii, $r(\tilde{\theta}), r(\tilde{\theta} + \delta\theta)$.

Theorem 2. *Let Ω be the internal cell space of a cell whose radius is is given by $\mathbf{r} : \mathcal{I} \times \Theta \to \mathcal{R}$. Further, let the perimeter length of the cell be given by $I_c = \int\limits_{\partial\Omega} \mathbf{r}(t,\theta)\, d\sigma_{\partial\Omega}$, where $\sigma_{\partial\Omega}$ is a surface element on $\partial\Omega$, and let $\widetilde{I}_c$ be given by the numerical approximation*

$$\widetilde{I} = \sum_{\tilde{\theta}\in\{0,\delta\theta,\ldots,2\pi-\delta\theta\}} \delta\theta \cdot \left(\left(\min(r(\tilde{\theta}), r(\tilde{\theta}+\delta\theta))\delta\theta\right)^2 + \left|r(\tilde{\theta}) - r(\tilde{\theta}+\delta\theta)\right|^2\right)^{\frac{1}{2}}.$$

Then, for a discrete step length, h, the error, E_L, for this approximation is of order $\mathcal{O}(h^2)$ and is given explicitly by

$$E_L \leq \int\limits_{\partial\Omega} \left[\frac{h^2}{2}\frac{\partial^2}{\partial\theta^2}\mathbf{r}(\theta_i + \eta) + \mathcal{O}(h^3)\right] d\sigma_{\partial\Omega}$$

Proof. Begin by noticing that our approximation is given precisely by the length of the line connecting the points $\mathbf{r}(\theta_i)$ and $\mathbf{r}(\theta_i + h)$ such that

$$\tilde{\mathbf{r}}(\eta) = \frac{\mathbf{r}(\theta_i + h) - \mathbf{r}(\theta_i)}{h}\eta + \mathbf{r}(\theta_i) \tag{17}$$

for $\eta \in (0, h)$ and centred around the point θ_i and where we are interested in values in the interval $(\theta_i, \theta_i + h)$.

Further, write the analytic function as the Taylor series

$$I_c(\theta_i + \eta) \approx \mathbf{r}\left(\theta_i + \eta\right) + \eta\frac{\partial}{\partial\theta}\mathbf{r}(\theta_i + \eta) + \frac{\eta^2}{2}\frac{\partial^2}{\partial\theta^2}\mathbf{r}(\theta_i + \eta) + \mathcal{O}(\eta^3) \tag{18}$$

then from the intermediate value theorem, we can choose η such that it satisfies

$$\frac{\partial}{\partial\theta}\mathbf{r}(\theta_i + \eta) = \frac{\mathbf{r}(\theta_i + h) - \mathbf{r}(\theta_i)}{h}\,. \tag{19}$$

Next, we take the difference between the two line integrals to find the analytic error in our approximation

$$\begin{aligned} E_L = \int\limits_{\partial\Omega} \left[\mathbf{r}\left(\theta_i + \eta\right) + \eta\frac{\partial}{\partial\theta}\mathbf{r}(\theta_i + \eta) + \frac{\eta^2}{2}\frac{\partial^2}{\partial\theta^2}\mathbf{r}(\theta_i + \eta) + \mathcal{O}(h^3)\right] d\sigma_{\partial\Omega} \\ - \int\limits_{\partial\Omega} \left[\frac{\mathbf{r}(\theta_i + h) - \mathbf{r}(\theta_i)}{h}\eta + \mathbf{r}(\theta_i)\right] d\sigma_{\partial\Omega} \end{aligned} \tag{20}$$

and since the linear terms for the Taylor expansion and the approximation (19) describes straight lines between two equidistant points, their magnitudes are equal. Therefore, considering that we have $h \geq \eta$, we obtain the maximal error bound

$$E_L \leq \int\limits_{\partial\Omega} \left[\frac{h^2}{2}\frac{\partial^2}{\partial\theta^2}\mathbf{r}(\theta_i + \eta) + \mathcal{O}(h^3)\right] d\sigma_{\partial\Omega}\,. \tag{21}$$

4 Results and Conclusions

In order to attempt the sorting experiment, we began with high affinity cells as the outer cells of a cellular Bravais lattice and low affinity cells in the centre, repeating the results of Graner *et al.* [5] (*data not shown*), which provided some base validation of the model. Counterintuitively, cells who have high cell-cell binding coefficients quickly separate into a web like structure whereas low binding constant scenarios tend to instead form a 2-dimensional hexagonal lattice.

In our second experiment we wanted a testable scenario to measure the migration of simulated cancerous cells through the ECM. For this we chose the scenario of microtracks since this presents 2 unique and measurably distinguishable scenarios in which to place our cells. We endow each with a polarisation of $\theta_p = 0$ and with the initial conditions $r^0(\theta) = \text{const.}$ such that they are represented as circular cells in the 2D domain. Working with a normalised 2D domain

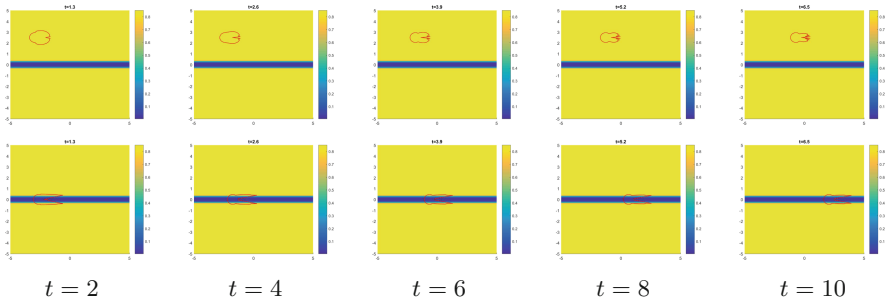

Fig. 1. Snapshots of simulated cells migrating through the ECM for the initial condition for the nucleus of the cell given within the ECM itself (*top*) or within an artificial microtrack (*bottom*) at times $t' \in \{2, 4, 6, 8, 10\}$.

$\mathcal{D} = [0, 1]^2$, parameter values were estimated and rescaled from experimental data [7] or approximated, in the case of cell-cell adhesion.

The first thing to notice is that although the membranes of cells within the microtracks start partially submerged in the ECM, they retract their membranes and conform entirely to the width of the microtrack (Fig. 1 *bottom*), as in the biological case [2]. Moreover, elongation in the microtrack cell is marked compared with those who remain within the ECM (Fig. 1).

Travel through the ECM also appears to be more conducive to the extension of lamellipodia (Fig. 1 *top*), whereas travel through the microtrack appears to be more conducive to the extension of longer, thinner, and more directive filopodia (Fig. 1 *bottom*). Not only this but the heterogeneity of the environment, alone, is sufficient to give rise to differing rates of travel within or without microtracks. Moreover, for increasing ECM density, one observes a decrease in velocity for cells within the ECM but no such changes in velocity for those within the microtrack (Fig. 2), which closely aligns with the results of *in vitro* experimentation [2].

Beyond the maximum time displayed ($t > 10$) these cells proceed to the right hand boundary and return to a more circular shape and lie dormant on this boundary *ad infinitum*. This is an artefact of the experiment, in that cells in this experiment have a fixed polarisation and are incapable of travelling in their assigned directions. In the following experiment we lifted this constraint.

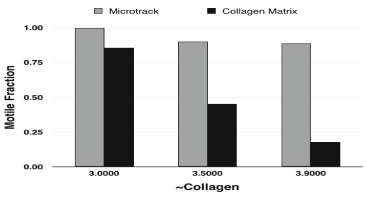

Fig. 2. Results of *in silico* microtrack experiments from the numerical simulations (*right*) and corresponding to those exemplar experiments in Fig. 1.

Our final experiment involves the interaction between two different metabolic phenotypes of cell: Highly proliferative, non-invasive ($\text{MITF}^{\text{HIGH}}$) cells and highly invasive, non-proliferative (MITF^{LOW}) cells. We begin with a heterogeneous distribution of v_1 and $v_2(t, x) = 0$. $\text{MITF}^{\text{HIGH}}$cells are attracted to v_2 but not v_1 and MITF^{LOW}cells are attracted to v_1 but not v_2 and convert $v_1 \to v_2$ [4]. Furthermore, to begin the experiment, we generated a random polarisation for each cell.

Injection of $\text{MITF}^{\text{HIGH}}$cells, alone (and in the absence of mitosis), reveals an extremely non-invasive behaviour with dominating cell-cell adhesive dynamics (Fig. 3 *top*). Injection of MITF^{LOW}cells, alone, one observes a highly invasive dynamic (Fig. 3 *middle*). Co-injection of the two disparate populations displays a mixture of behaviours between cell-cell binding and cell-ECM motility and one observes a co-invasion of $\text{MITF}^{\text{HIGH}}$cells in the wake of invading MITF^{LOW}cells (Fig. 3 *bottom*). Again, one can identify the production of filopodia by cells who have elongated upon the heterogeneous substrate for invasion (Fig. 3).

The qualitative results of this experiment were not significantly effected by the random initial polarisations of the cells. In the short term ($t \leq 200$) cellular automata mimic the behaviour of *in vivo* cells [4], with $\text{MITF}^{\text{HIGH}}$cells clustering and MITF^{LOW}cells dispersing, in isolation, and some intermediate behaviour, otherwise. These times were chosen to be indicative of the overall behaviour as, in the long term ($t > 200$), those cells who have not yet dispersed at $t = 200$ will continue to cluster, whilst those who have dispersed will find some steady state position at the boundary of the domain $t \to \infty$. Again, these behaviours show close conformity with *in vivo* experiments [4], assuming that those on the boundary of the domain would otherwise continue to invade.

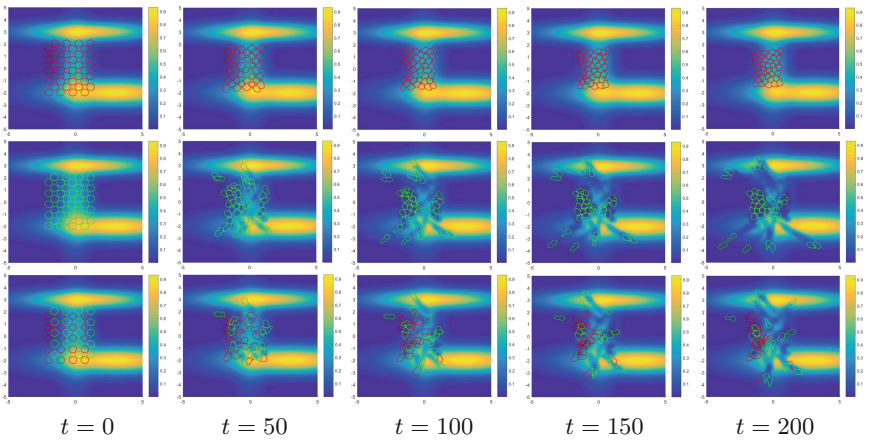

Fig. 3. Experimental *in silico* injection of *red* $\text{MITF}^{\text{HIGH}}$cells (*top*); *green* MITF^{LOW}cells (*middle*); or both cell types (*bottom*) onto a heterogeneous density function for v_1 coloured *blue* through *yellow*, at time points $t \in \{0, 50, 100, 150, 200\}$. (Color figure online)

We have derived a modelling framework to solve problems which previous frameworks [5,10] were unable to approach. Errors for the numerical implementation of estimates for these models are small and, as such, allow one to be confident in their predictive power. Moreover, the introduction of low-error approximations to this framework allow for a fast model execution time. This novel modelling framework has also shown practical promise; recreating the cell sorting experiment before predicting the outcomes of biological microtrack [2] and co-invasion [4] experiments. Moreover, this model may explain emergent phenomena, such as cellular elongation and filo- or lamellipodia extension, which could be explained through simple physical interactions between the cellular membrane and the homo- or heterogeneous ECM. Future work should aim to extend this model through the addition of microscale boundary interactions and look to explore more complex biological phenomena.

This cellular automata model could also be useful in other environments where one requires a nuanced interaction between automata and their contexts. This can be achieved either through the method of implementation employed above, for entirely nonlocal interactions, or through treating the cellular membrane as a domain boundary and utilising a kernel to vary the impact across the domain, allowing diverse interactions between automata and their contexts. Obvious applications of this framework arise in cellular biology but one can also envisage application in game theory and financial markets, where individuals (automata) will or must take into account their environment (the context) to varying degrees.

References

1. Buxboim, A., Ivanovska, I.L., Discher, D.E.: Matrix elasticity, cytoskeletal forces and physics of the nucleus: how deeply do cells 'feel' outside and in? J. Cell Sci. **123**(Pt 3), 297–308 (2010)
2. Carey, S.P., et al.: Comparative mechanisms of cancer cell migration through 3D matrix and physiological microtracks. Am. J. Physiol. Cell Physiol. **308**(6), C436–C447 (2014)
3. Carpen, O., Pallai, P., Staunton, D.E., Springer, A.T.: Association of intercellular adhesion molecule-1 (ICAM-1) with actin-containing cytoskeleton and -actinin. J. Cell Biol. **118**(5), 1223–1234 (1992)
4. Chapman, A., del Ama, L.F., Ferguson, J., Kamarashev, J., Wellbrock, C., Hurlstone, A.: Heterogeneous tumor subpopulations cooperate to drive invasion. Cell Rep. **8**, 688–695 (2014)
5. Graner, F., Glazier, J.A.: Simulation of biological cell sorting using a two-dimensional extended Potts model. Phys. Rev. Lett. **69**(13), 2013–2016 (1992)
6. Herman-Bausier, P., El-Kirat-Chatel, S., Foster, T.J., Geoghegan, J.A., Dufrêne, Y.F.: Staphylococcus aureus fibronectin-binding protein a mediates cell-cell adhesion through low-affinity homophilic bonds. mBio **6**(3), e00413–e00415 (2015)
7. Johnson, C.P., Tang, H.Y., Carag, C., Speicher, D.W., Discher, D.E.: Forced unfolding of proteins within cells. Science **317**(5838), 663–666 (2007)
8. Kraning-Rush, C.M., Carey, S.P., Lampi, M.C., Reinhart-King, C.A.: Microfabricated collagen tracks facilitate single cell metastatic invasion in 3D. Integr. Biol. **5**(3), 606–616 (2013)

9. Nyman-Huttunen, H., Tian, L., Ning, L., Gahmberg, C.G.: α-Actinin-dependent cytoskeletal anchorage is important for ICAM-5-mediated neuritic outgrowth. J. Cell Sci. **119**(Pt 15), 3057–3066 (2006)
10. Turner, S., Sherratt, J.A.: Intercellular adhesion and cancer invasion: a discrete simulation using the extended Potts model. J. Theor. Biol. **216**, 85–100 (2002)
11. Zaman, M.H., Kamm, R.D., Matsudaira, P., Lauffenburger, D.A.: Computational model for cell migration in three-dimensional matrices. Biophys. J. **89**(2), 1389–1397 (2005)